The Transient Liquid Crystal Technique Employed for Sub- and Transonic Heat Transfer and Film Cooling Measurements in a Linear Cascade

Hans Reiss, Albin Bölcs
Laboratoire de Thermique Appliquée et de Turbomachines (LTT)
Swiss Federal Institute of Technology
CH-1015 Lausanne, Switzerland

Uwe Drost
ABB Power Generation Ltd.
CH-5400 Baden, Switzerland

ABSTRACT

An experimental system based on the transient liquid crystal technique is presented, suitable to provide both aerodynamic and heat transfer data on film-cooled airfoil models in sub- and transonic flow regime.

The experimental set-up consists of a linear cascade test facility which can be operated at transonic flow conditions, and exit Reynolds numbers up to 1.6e6 based on the chord length, and high free-stream turbulence level. The centerblade of the cascade is mobile and can be withdrawn from the channel to be preconditioned, and then rapidly exposed to the flow during the transient test.

The data analysis as well as the measurement equipment is described, with a special focus on the computerised image processing system that is used to capture the liquid crystal signal. The transient technique was directly compared to the adiabatic wall technique and showed good agreement. Some special topics, as the validity of the method in the near-hole region, and the assessment of the coolant temperature are addressed.

Sample results of heat transfer on an uncooled blade model, as well as an airfoil with film cooling are shown.

NOMENCLATURE

A	[m^2]	surface area
c_p	[J/kgK]	specific heat at constant pressure
d	[mm]	leading edge, diameter, hole diameter
D	[mm]	cylinder diameter
DR	[-]	coolant-to-gas density ratio ρ_c/ρ_g
G	[-]	bulk blowing ratio $u_c\rho_c/u_g\rho_g$
I	[-]	bulk momentum flux ratio $u_c^2\rho_c/u_g^2\rho_g$
L	[m/s]	cooling hole length
L_x	[m]	longitudinal integral lengthscale
M	[-]	Mach number $u/(\kappa RT)^{0.5}$
n	[-]	summation index
p	[Pa]	pressure
q	[W/m^2]	specific heat flux
R	[J/kg/K]	ideal gas constant
Re	[-]	Reynolds number (uL)/ ν
R_a,R_z,R_t	[µm]	surface roughness parameters (DIN4768)
r_0	[-]	recovery factor
T	[K]	temperature
t	[s]	time
Tu	[%]	turbulence intensity
u	[m/s]	velocity
x	[m]	model depth

GREEK

α	[$W/(m^2K)$]	local heat transfer coefficient
β	[°]	spanwise inclination angle
γ	[°]	surface angle, exit location angle
η	[-]	film cooling effectiveness
φ	[°]	streamwise inclination angle
ρ	[kg/m^3]	density
τ	[-]	summation index
µ	[Ns/m^2]	dynamic viscosity
ν	[m^2/s]	kinematic viscosity
κ	[-]	isentropic coefficient c_p/c_v
λ	[J/mK]	thermal conductivity
Λ	[m^2/s]	thermal diffusivity $\lambda/(\rho c_p)$
Φ	[-]	overall effectiveness

SUBSCRIPTS

aw	adiabatic wall
c	coolant

Presented at the
14th Bi-annual Symposium on Measurement Techniques in Transonic and Supersonic Flow in Cascades and Turbomachines
University of Limerick, 3-5 Sept. 1998

f	film cooling
g	main stream gas
i	initial
r	recovery
s	static conditions, surface
t	total conditions
0	reference, cooling hole base

INTRODUCTION

Heat transfer plays a crucial part in the development of turbine blades. Gas temperatures in the first stages of the turbine may largely pass metal melting temperatures, and extensive cooling of these components - the first vanes and blades in particular - is absolutely necessary. Usually a combination of internal convection cooling and film cooling is employed. They have to be designed for high performance, long life cycles and safe operation despite being subjected to high thermal loadings of an engine environment. High uncertainties for the local heat transfer persist and therefore an exact prediction of resulting material temperatures – key parameter for thermal blade design - is difficult. It is therefore desirable to have detailed knowledge of local heat transfer rates in complex flow situations such as film cooled turbine blades.

The experimental set-up presented here is able to provide complementary data of heat transfer and flowfield around film-cooled turbine blades under transonic conditions. The transient liquid crystal technique, that has been previously used for flat plate and cylinder-in-crossflow experiments by (Drost and Bölcs 1996) and (Hoffs, Drost et al. 1997) is now described for transonic film cooling and heat transfer experiments on turbine airfoils. The method allows to obtain detailed surface distributions of both local heat transfer coefficients and film cooling effectiveness for film-cooled airfoils, which enables to fully predict the resulting heat loads under real-engine conditions.

Basic Principle

The Transient Liquid Crystal Technique consists of provoking a heat pulse into the test specimen by exposing a preconditioned model rapidly to an air flow at a different temperature level, and then monitoring the evolution of the surface temperature during such a transient experiment via thermochromic liquid crystals as shown in Fig. 1.

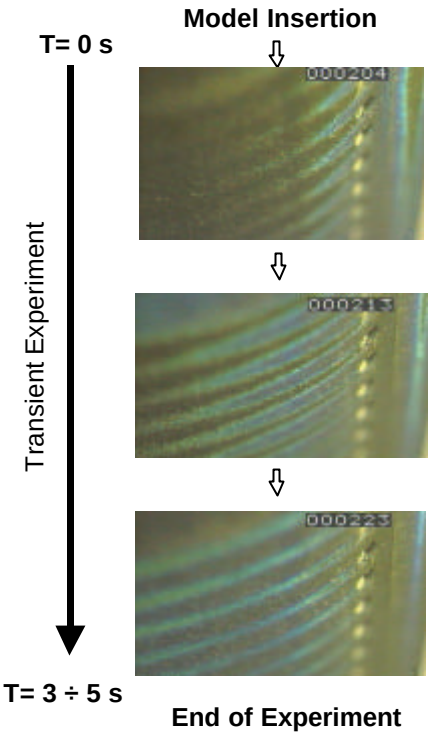

Fig. 1 – Liquid Crystal Thermography for a Transient Heat Transfer Experiment

From the time it takes between model exposure and a point at the surface reaches a certain temperature value, one can conclude on the local heat transfer rate, and on the effective gas temperature at this point. This is an optical measurement technique and yields a high spatial resolution, which makes it applicable to highly complex film cooling schemes, including multiple row injection and shaped holes.

THEORY AND DATA ANALYSIS

The local heat flux onto a film-cooled surface can be written as

$$q = a_f (T_{aw} - T_w) \tag{1}$$

where the driving temperature difference for the definition of α_f is the adiabatic wall temperature T_{aw} (which is the effective gas temperature at the wall) minus the surface temperature of the model. T_{aw} is unknown and depends on the temperatures of main stream and injected coolant gas, and on the mixing between jets and main flow. It can be written in dimensionless form as film cooling effectiveness

$$h = \frac{T_{aw} - T_{rg}}{T_{tc} - T_{tg}} \tag{2}$$

expressing how closely T_{aw} approaches the coolant injection temperature. In this definition, the respective total temperatures appear in the denominator, although these are not encountered in the actual injection situation. These were chosen in order to make the denominator independent from the flow field, in particular the cooling injection velocity. Therefore, results with different blowing ratios can more easily be compared. Both unknowns α_f and η are a function of the aerodynamic flow field alone and do not depend on the actual choice of the temperature values, as long as constant gas properties

are supposed (Vedula and Metzger 1991).

The data analysis is based on the theory of one-dimensional transient heat conduction into a semi-infinite solid. The governing differential equation for the temperature evolution of the solid is

$$\frac{\partial^2 T}{\partial x^2} = \frac{1}{\Lambda}\frac{\partial T}{\partial t} \tag{3}$$

with the initial condition $T(x,t)\big|_{t=0} = T_i$. It is supposed that, during an experiment, a heat pulse enters only a short distance into the model compared to its wall thickness, i.e. the model interior remains at initial temperature T_i for all times, and the temperature gradient $\partial T/\partial x$ is zero. This is formally expressed as the boundary condition for Eq. (3) as $\lim_{x\to\infty} T(x,t) = T_i$. This approach is only valid for relatively short measuring times smaller than a value t_{limit} which is a depends on the local wall thickness of the model and its thermal properties, according to (Schultz and Jones 1973)

$$t_{\lim it} = \frac{L^2}{16\Lambda} \tag{4}$$

As long as t stays below t_{limit}, the temperature change at the model back is inferior to 1% of the temperature change at model surface, and thus the assumption of semi-infinite solid can be considered as true. At the surface a convective boundary condition is imposed :

$$-l\left.\frac{\partial T(x,t)}{\partial x}\right|_{x=0} = a_f\left(T_{aw} - T(x,t)\right)\Big|_{x=0} \tag{5}$$

Eq. (5) represents an instantaneous step change of the effective fluid temperature at model surface from T_i to T_{aw}. Practically, a true step change for the main stream temperature can well be approximated by rapid exposure of the preconditioned model to the flow (Hoffs, Drost et al. 1997). However, this is not the case for T_{aw} since inevitably the coolant injection temperature varies gradually during a transient experiment due to internal heat exchange which occurs in the supply tubings, the plenum and particularly in the cooling holes inside of the pre-conditioned model. Thus, the adiabatic wall temperature becomes a function of time. This is accounted for by approximating the measured coolant injection temperature with a power series of typically 4th to 5th order as

$$T_{tc}(t) = \sum_{n=0}^{N} A_n \frac{t^n}{\Gamma(n+1)} \tag{6}$$

Employing this transient coolant temperature, the Laplace transform method yields an analytical solution for the temperature evolution at x=0 as previously described by (Drost, Bölcs et al. 1997)

$$T_w - T_i = (T_{rg} - hT_{tg} - T_i)\left[1 - e^{b^2}erfc(b)\right] - h\sum_{n=0}^{N}\left\{A_n\left(\frac{k}{a_f}\right)^{2n}\left[e^{b^2}erfc(b) - \sum_{t=0}^{2n}((-2b)^t i^t erfc(0))\right]\right\} \tag{7}$$

with $k = \frac{l}{\sqrt{\Lambda}} = \sqrt{r\,lc_p}$ and $b = \frac{a_f\sqrt{t}}{k}$

Eq. (7) contains the two unknowns α_f and η. In order to solve for α_f and η, a multiple-regression analysis is applied: A number of 6 to 8 transient experiments is conducted at identical aerodynamic and thermal conditions but with varying the coolant temperature. The result is a set of curves describing the wall temperature rise for a given surface position, as indicated in Fig. 2. Since a single layer of narrow band liquid crystals is used, one "event" can be detected per chosen hue value and test, that is when the surface point passes at the corresponding liquid crystal temperature T_{LC}. Eq. (7) is then least-square fitted to the ensemble of points $(t,T_w=T_{LC})_i$ yielding both unknowns α_f and η.

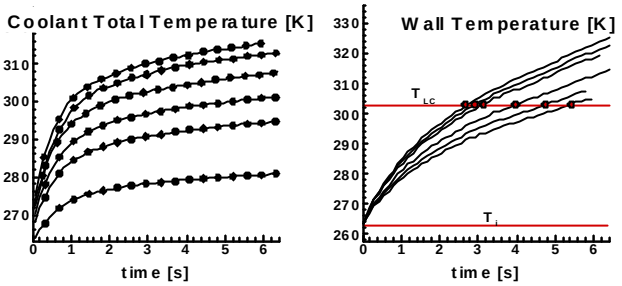

Fig. 2 – Variation of Coolant and Wall Temperatures for a Test Ensemble

Measurement Uncertainties

Compared to data evaluation using the minimum of only two experiments, the advantage of the 'overdetermined' method using the regression analysis is that the uncertainties can be reduced. Taking into account the existing uncertainties for the individual quantities that are directly measured, the data analysis yields an uncertainty on the heat transfer coefficient of about 6%, and on the film cooling effectiveness of 4% (for η=0.3) to 10% (for η=0.1).

TEST FACILITY AND INSTRUMENTATION

Linear Cascade Test Facility

Fig. 3 shows a sketch of the partly unmounted wind tunnel holding the test section with 5 blades. The flow channel is 99mm wide, and the blade pitch is fixed to 64mm. For this study, straight or contoured endwalls may be used. In the first case the resulting flow field is essentially 2-dimensional. Depending on the actual blade profile used, an aspect ratio (span/pitch) of about 1.5 are achieved. Two tailboards and bypass vanes are installed for adjustment of flow conditions, and in particular to assure good periodicity within the two center passages of the cascade. Up to 10 kg/s air can be supplied continuously to the test stand at pressure levels of up to 2.5 bar, allowing to operate the cascade at sub- and transonic flow conditions. Maximum exit Reynolds numbers of 1.7e6 (based on a chord length of about 80mm) can be achieved. The free stream turbulence level can be varied between Tu=5.5 and 10% by adding different types of turbulence grids to the test section entry.

Coolant Gas Supply

Either air or foreign gas is provided as secondary fluid to the film-cooled model. The coolant mass flow rate is controlled via sonic blockage using a reservoir with choked orifice, allowing an accurate adjustment of the blowing ratio. During the transient tests, the actual flow rate is continuously measured with a laminar flow element. The coolant temperature is pre-set with electrical heaters.

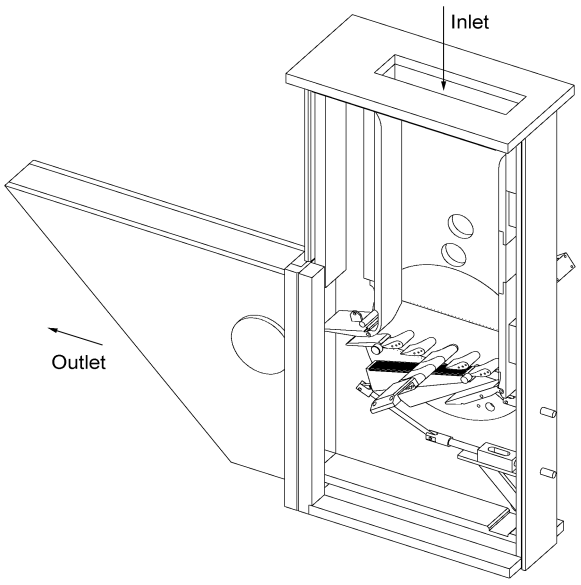

Fig. 3 – Linear Cascade Wind Tunnel

The heat transfer test blade, situated in the center of the cascade, can be removed from the flow for preconditioning prior to the transient experiment, and replaced by an aerodynamic dummy blade. The insertion mechanism is shown in Fig. 4 (preconditioning position on top, measurement position on below). The mechanism is activated via a computer-controlled pneumatic cylinder, and insertion time is below 0.1s.

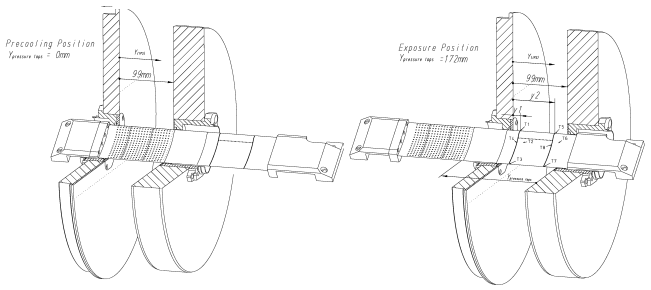

Fig. 4 – Rapid Insertion Mechanism for Blade Model

A cut through the channel center is depicted in Fig. 5 showing the two circular disks on the left and the right with integrated sealing boxes. The centerblade is sliding in a tightly fit teflon guidance on the 'dummy' one side in order to avoid misalignment of the blade with the neighbouring blades, and to prevent bending of the centerblade by the aerodynamic forces. Pneumatic seals, consisting of inflatable silicon tubes close tightly around the blade and add additional guidance and centration. They are synchronised with the insertion mechanism, i.e. they are automatically deflated during any blade movement.

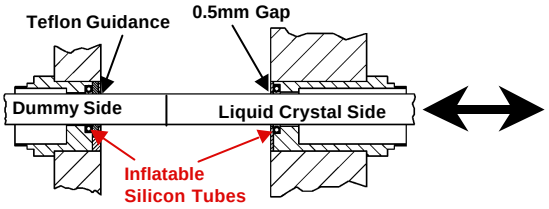

Fig. 5 – Pneumatic Seals for Mobile Centerblade

Instrumentation

Main stream flow conditions are determined by a total pressure probe upstream of the test section which is completely retrieved from the channel before an actual heat transfer measurement in order not to disturb the flow field by the wake of the probe. Flow temperature is taken with a total temperature probe in settling chamber upstream. The test section itself (shown in Fig. 6) is equipped with a series of static pressure taps in the side walls up- and downstream of the cascade.

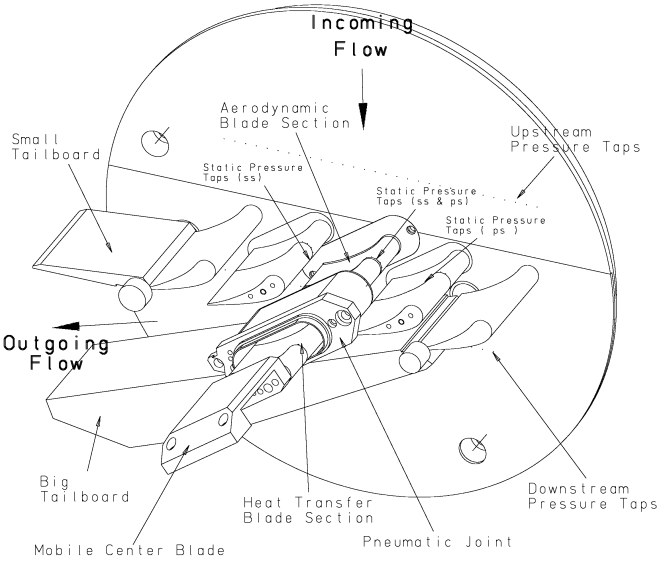

Fig. 6 – Linear Cascade Test Section

Static pressure taps are distributed around the center and the two adjacent blades at mid-span. The tap positions are indicated in Fig. 7. By comparing static pressure profiles of pressure- or suction side on the centerblade with the pressure- or suction side on the respective neighbouring blade, the periodicity of the flow can be verified. As shown on the right of Fig. 7 the centerblade is assembled from a 'dummy' portion carrying the pressure taps and a machined-on reference grid, and a heat transfer section. Apart from transient heat transfer measurements, the insertion mechanism is also used to scan the pressure field across the channel by traversing it in small increments in spanwise direction, yielding full pressure distributions on the center blade. Additionally, aerodynamic losses of the over the cascade can be determined with downstream traverses of aerodynamic probes (not explicitly shown in the sketch).

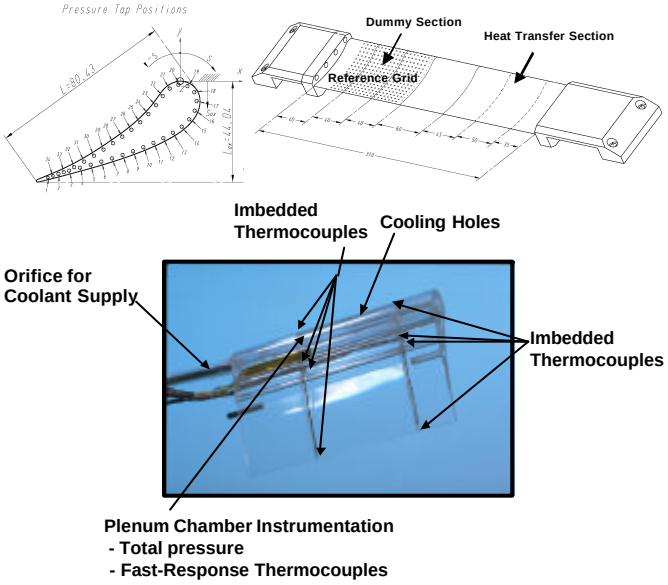

Fig. 7 – Mobile Centerblade Instrumentation

A photograph of the heat transfer blade section can be seen in Fig. 7. It holds a number of 6-8 embedded small thermocouples that are arranged in two planes, yielding the initial temperature of the model. Depending on the film cooling configuration of the respective specimen, one or two plenum chambers with cooling orifices are machined into the model, each of them containing a total pressure and a fast-response thermocouple probe in about the middle of the plenum volume. It was shown that the exact position of these probes does not influence the measurement, which confirms the hypothesis of having coolant total conditions in the plenum.

The model surface is coated with a black ink backing, followed by commercial narrow-band encapsulated thermochromic liquid crystals (Hallcrest™, U.K.) and a thin layer of transparent binder on top, in order to protect them from early damaging. A fine airbrush is used for application, and the coating is polished for a smooth surface with good repeatability. Typically, a surface roughness of R_z=9±1.5 µm, R_a=2.4±0.5µm, and R_t=15±2.7µm is achieved.

IMAGE PROCESSING SYSTEM

Hardware

The colour play of the liquid crystals is captured with several miniature colour CCD cameras (TELI CS 5130, 6000 ; resolution 752x582 pixels) through small access windows in the channel side walls. The small size of the separate camera heads (diameter 12mm, length 40mm) simplifies camera placement. At least three camera views are needed in order to capture the entire blade surface, and some additional positions are usually chosen to zoom in on regions of interest, as for example the near hole region of injection stations. The model surface is illuminated through the side walls with endoscopic cold-light sources. An image processing computer (ELTEC Eurocom 7, CPU 68040, 16MB RAM, 2.6 MB Memory) is employed for real-time treatment of the video signal.

Hue-Capturing Technique

The RGB image signal is viewed and recorded with standard video devices for control purposes, however the actual data treatment is directly done with the image processing computer. For that purpose, the RGB signal is first transformed into a hue-saturation-intensity signal. Before actually storing the image sequence into the RAM, all but some user-specified colour bands (corresponding to a given hue value with a defined bandwidth) are filtered out, which yields a considerable reduction of the data. Typically three colours bands are chosen, two for temperature monitoring (green and cyan, which proved to be most clearly detectable), and a third colour band (red) used as a trigger to indicated the exact moment of model insertion. The liquid crystals are calibrated with the blade in the channel at very low speed flow conditions, with the cameras and light sources readily installed, and the hue-filtering parameters configured. By slowly rising the main stream temperature from ambient values appearance of a certain hue-value in the filtered signal is directly related to the temperature given by the closest embedded thermocouple. The temperatures corresponding to the two chosen colours green and cyan are approximately 0.5° apart. An accuracy of the calibration of ±0.15°C for each colour can be achieved. The influence of view angle or irregular illumination, effects which must be taken into account when using wide-band liquid crystals, can therefore be neglected.

Two camera signals can be treated in parallel, i.e. in interlaced mode, as schematically shown in Fig. 8. The frames at beginning of a sequence contain the trigger signal (which is the colour of the reference grid, and which does not appear in the liquid crystal colour play). The disappearance of this trigger defines the moment of model exposure. It is with this trigger signal that the image sequence is co-ordinated in time with other acquired unsteady measurement data (thermocouples, mass flow, etc.). The subsequent images show the passing colour bands, whereas the rest of the image is black. After the measurements, the image sequence files are transferred to workstation for data analysis as described above.

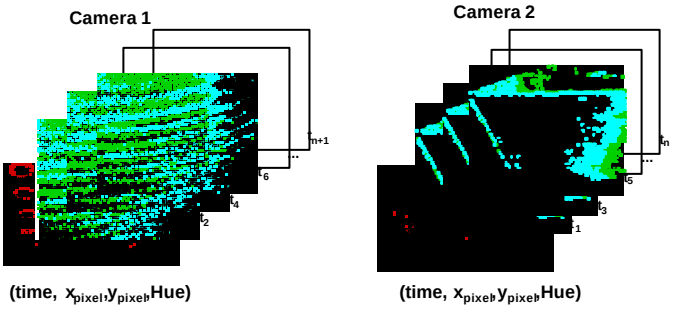

Fig. 8 – Double Camera-Real Time Acquisition of Filtered Image Sequence

Co-ordinate Transformation

The camera sequences inevitably contain deformed images, and therefore a co-ordinate transformation has to be done relating a given pixel position of the image to a point on the model surface. The procedure is summarised in Fig. 9 : An image of the reference grid on the dummy blade portion is acquired for each of the camera views. The grid points are then used to define a set of spline interpolation functions ; based on this interpolated grid, each pixel position is related to its corresponding surface position. The transformation is stored in form of a transformation matrix, which is subsequently applied to the entire image sequences, prior to event separation.

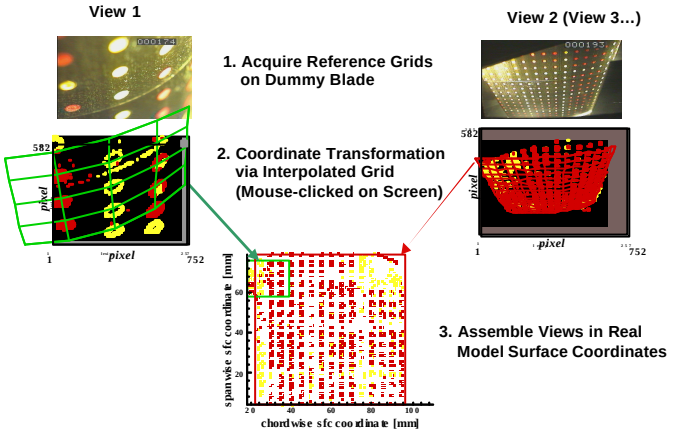

Fig. 9 – Image-to-Model-Co-ordinate Transformation

Event Separation

The time lap between model insertion and actual event appearance has to be extracted from the image sequences, in principle for each chosen colour band and position. However, due to the nature of the video image, which contains noise and may not be complete (i.e. missing signal at some locations where no liquid crystal signal was detected), a separate treatment of every image pixel is not practical. Instead, a number of pixels are treated together, by subdividing the model surface into a regular grid, and treating together the ensemble of pixels that come to lie within such a grid cells after the co-ordinate transformation. The cell size can be defined according to the camera view and the quality of the crystal signal. For example a spatial resolution down to 0.1mm (real surface co-ordinates) can be obtained for a zoomed-in view around film cooling holes.

An averaging procedure in both time and space is then applied to actually sort out the 'events'*(time, T_{LC})*: a hue signal needs to appear at a surface position as well as neighbouring positions, over a number of consecutive images in order to be considered as an event. The result of the image processing is a number of events for each surface position. This information is passed-on to the data analysis as explained above.

EXPERIMENTAL PROCEDURE

The test facility runs at steady state conditions. Main stream temperature is adjusted to 60-65°C. Prior to the heat transfer test, the cylinder model is being preconditioned to an initial temperature of about –15°C. In order to achieve the desired spread of injection temperatures of an ensemble of tests, it is necessary to precondition the coolant supply chain (tubings, valves, etc.). Thus the supply system is rinsed up to the actual orifice to the model with preconditioned air. Only very shortly before transient test start, the coolant reservoir is switched on. When the model is inserted, a mechanically activated valve switches the coolant flow from bypass to the plenum. The transient total temperature in the plenum is measured with fine, fast-response thermocouples residing in the plenum center, and the coolant total pressure is acquired with a pressure tap (see also Fig. 7). This transient data is stored and processed together with the image sequences.

The actual coolant exit temperature $T_{tc}(t)$ that enters into the data analysis according to Eq.(5) is determined via an isentropic calculation, based on the measured total conditions in the plenum and the static pressure at hole exit. The latter is interpolated from the pressure measurements on the blade surface.

SPECIAL CONSIDERATIONS ABOUT THE NEAR-HOLE REGION

A special question of the measurement technique arises when applied to film cooled models : the influence of 3-dimensional conduction effects. Numerical simulations of small segment of the model containing a single cooling hole have been carried out in order to estimate the error. For this calculation, typical values of initial and hot gas temperatures where chosen, and a known constant heat transfer coefficient of 600W/m^{2}K was applied as outer boundary condition. Within the cooling hole, a fixed distribution of heat transfer coefficients from heat exchanger correlations was used, and a coolant mass flow was defined representative for typical blowing ratios. Fig. 10 clearly shows the deformation of the entering heat pulse due to the hole. The numerically calculated surface temperature evolution was then subjected to 'classical' data analysis based on the 1-dimensional semi-infinite heat conduction equation for re-calculation of the heat transfer coefficient.

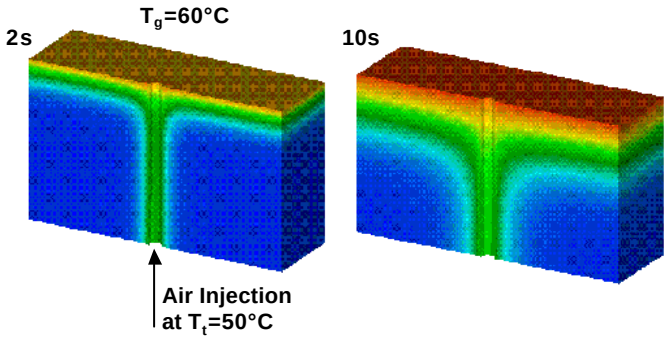

Fig. 10 - 3D Numerical Simulation of Entering Heat Pulse around a Cooling Hole

The results along the centerline of the block is shown in Fig. 11 . Each curve was using the instantaneous surface temperature distribution at the given time value. It is apparent that - far away from the hole, very good agreement with the imposed value of 600W/mK2 exists, whereas close to the hole the heat transfer is overestimated. The error increases with shorter the 'measurement time'. At positions further then one hole diameter away, however, the error lies under 10%. It can therefore be concluded that the influence of 3-D conduction is limited to the very near-hole region, whereas the data analysis gives valid results for the rest on the test specimen.

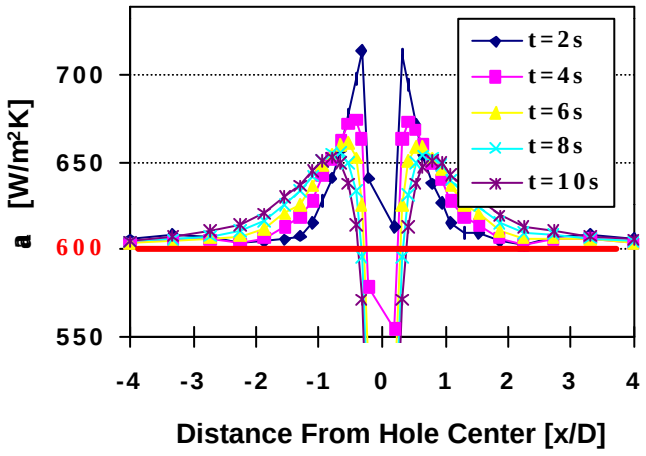

Fig. 11 – Recalculated Heat Transfer Coefficient Based on 1D Data Analysis

ASSESSMENT OF COOLANT INJECTION TEMPERATURE

Also related to the validity of the technique is the issue of transient internal heat transfer within the plenum chamber and the film cooling holes which inevitably occurs. The analysis is based on the assumption that the actual exit coolant temperature is known, however the hole dimensions do not allow to measure it directly. As mentioned, an isentropic calculation is used to calculated exit conditions form total conditions in the plenum, and internal heat transfer is neglected.

A similar numerical simulation of the transient heat exchange in the near-hole region has been done, this time focusing on the heat pick-up of the coolant gas from the preconditioned cooling hole walls. Fig. 12 shows the coolant bulk temperature along the cooling hole for different times. The error on the coolant exit temperature due to internal heat exchange depends strongly on the actual coolant temperature of the respective test. A 'worst case' estimation employing a very long cooling hole, and the biggest expected gradient between coolant- and model initial temperature, yielded an error of less then 0.8°C which is considered negligible.

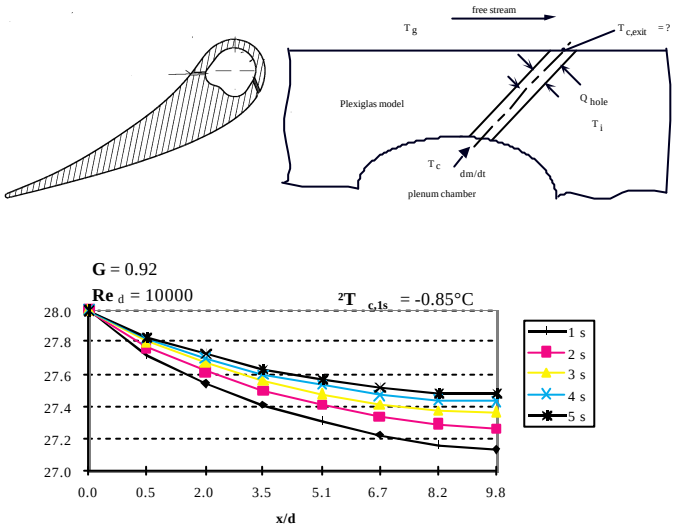

Fig. 12 – Calculated Evolution of Bulk Coolant Temperature Along Injection Hole

COMPARISON WITH THE ADIABATIC WALL METHOD

The transient liquid crystal technique has been compared to the adiabatic wall technique, which consists of exposing the model to the main flow, continuously injecting coolant gas at a given temperature and wait until the surface temperature is readily established. Here, the identical model was used as in the transient experiments. At the positions where the liquid crystal iso-lines appear, the film cooling effectiveness is calculated directly according to Eq.(2). Fig. 13 shows spanwise average effectiveness for the transient experiment and a number of steady state experiments, each of which yielded two data points. Excellent agreement between the transient and the adiabatic wall technique is obvious.

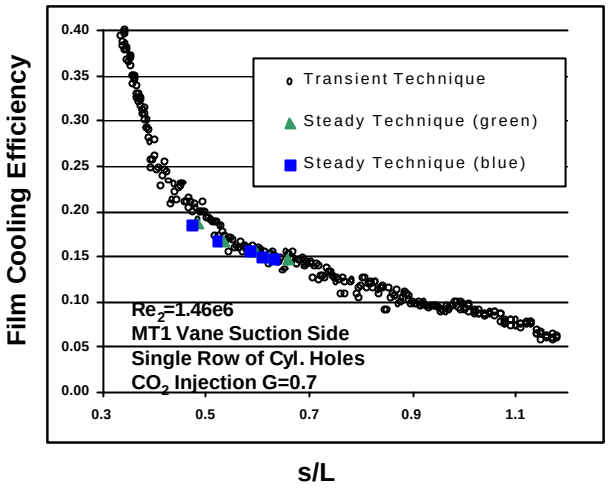

Fig. 13 – Film Cooling Efficiencies with Different Techniques

SAMPLE RESULTS

An airfoil model without film cooling (see Fig. 14) was investigated with respect to the boundary layer state: a case with undisturbed boundary layer, a case with the presence of cooling holes on the suction side at s/L=0.2, but zero injection, and the case of tripped boundary layer (taped-on wire at s/L=0.125). The spanwise average heat transfer coefficient in Fig. 15 clearly shows how the heat transfer is influenced by the boundary layer state.

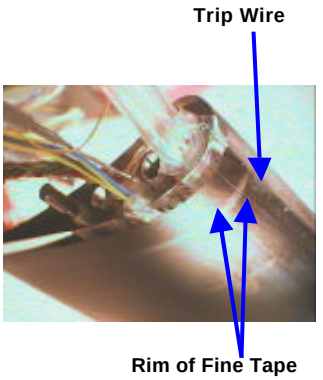

Fig. 14 . – Model Blade with Pasted Trip Wire

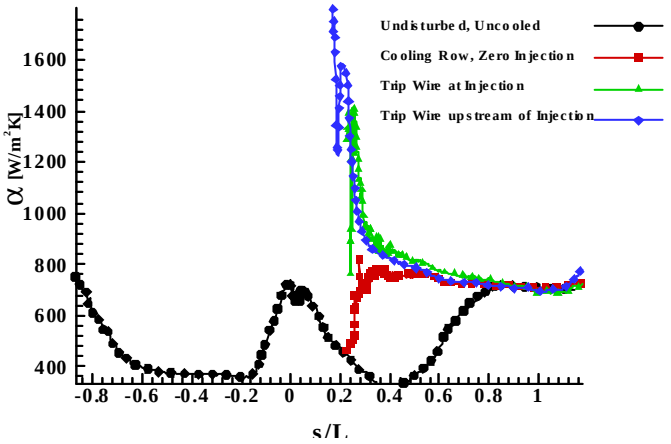

Fig. 15 – Spanwise Averaged Heat Transfer Distribution

To further illustrate the type of results that can be obtained with the liquid crystal technique, an example of detailed film cooling effectiveness on an airfoil suction side with film cooling is shown in Fig. 16. The surface distribution is assembled from an overall view of the suction side, and a zoom around some injection holes, yielding high resolution results.

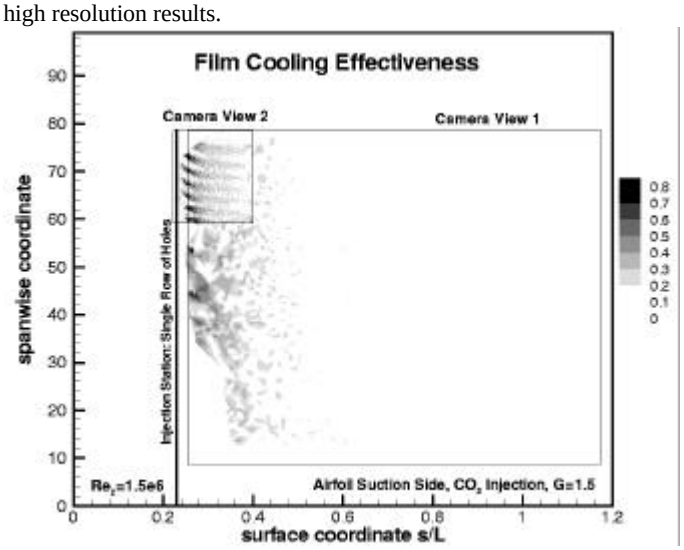

Fig. 16 – Effectiveness on Film-Cooled Airfoil Suction Side

CONCLUSIONS

The transient liquid crystal technique for heat transfer and film cooling measurement was described in this paper, allowing to gather detailed film cooling effectiveness and heat transfer coefficients. A test facility suitable for airfoil measurements with film cooling under transonic flow conditions was presented. Several practical aspects of the technique, such as crystal calibration, details of the image processing procedure and coolant temperature assessment were addressed. The transient technique agreed well with the adiabatic wall technique.

ACKNOWLEDGEMENTS

The transient liquid crystal technique was first set up within a research project subsidised by ABB Power Generation Ltd., Switzerland and the Nationaler Energie-Forschungs Fonds (NEFF-KWF), Switzerland. It is currently applied within the European research project TATEF under the BriteEuram 4th framework, and sponsored by the Swiss Government.

REFERENCES

Drost, U. and Bölcs, A. (1996). The Transient Liquid Crystal Technique Applied for the Investigation of Flat Plat and Showerhead Film Cooling, Measurement Techniques, Zürich.

Drost, U., Bölcs, A. and Hoffs, A. (1997). Utilization of the Transient Liquid Crystal Technique for Film Cooling Effectiveness and Heat Transfer Investigations on a Flat Plat and a Turbine Airfoil. IGTA, Orlando, Florida.

Hoffs, A., Drost, U. and Bölcs, A. (1997). An Investigation of Effectiveness and Heat Transfer on a Showerhead-Cooled Cylinder. IGTA, Orlando, Florida.

Schultz, D. L. and Jones, T. V. (1973). Heat Transfer Measurements in Short Duration Hypersonic Facilities NATO Advisory Group Aeronautical RD AGARDOGRAPH 165.

Vedula and Metzger (1991). A method for the simultaneous

determination of local effectiveness and heat transfer distributions in three-temperature convection situations.ASME paper 1991